






## Article

# Zaykovite, Rh<sub>3</sub>Se<sub>4</sub>, a new mineral from the Kazan placer, South Urals, Russia

Elena V. Belogub<sup>1\*</sup> , Sergey N. Britvin<sup>2,3</sup> , Vladimir V. Shilovskikh<sup>2</sup> , Leonid A. Pautov<sup>1,4</sup>, Vasilii A. Kotlyarov<sup>1</sup> and Elisaveta V. Zaykova<sup>1</sup>

<sup>1</sup>South Urals Federal Research Center of Mineralogy and Geoecology, Uralian Branch of Russian Academy of Sciences, Miass, 456317, Russia; <sup>2</sup>Saint-Petersburg State University, Universitetskaya Emb. 7/9, Saint Petersburg, 199034, Russia; <sup>3</sup>Nanomaterials Research Center, Kola Science Center of the Russian Academy of Sciences, Fersman Str. 14, 184209 Apatity, Russia; and <sup>4</sup>Fersman Mineralogical Museum of the Russian Academy of Sciences, Leninsky Pr. 18-2, Moscow, 115162, Russia

### Abstract

Zaykovite, ideally Rh<sub>3</sub>Se<sub>4</sub>, is a new mineral, the first natural rhodium selenide. It was discovered in the assemblages of platinum-group minerals from the Kazan gold placer, South Urals, Russia. The mineral occurs as crystals up to 40 μm in size within the grains of Pt<sub>3</sub>Fe alloy, in association with unnamed Pd–Sb–Te phase and Au–Pd alloy. In reflected light, zaykovite has a grey colour with bluish-greenish tint; it shows weak bireflectance and anisotropy. Reflectance values [ $R_{\max}/R_{\min}$  (%) for COM approved wavelengths (nm)] are: 30.1/29.3 (470), 32.2/31.0(546), 33.4/32.0(589) and 35.1/33.7(650). The chemical composition corresponds to the empirical formula (Rh<sub>2.26</sub>Pt<sub>0.46</sub>Ir<sub>0.25</sub>Ru<sub>0.01</sub>Pd<sub>0.01</sub>Fe<sub>0.01</sub>)<sub>Σ3.00</sub>(Se<sub>2.77</sub>S<sub>1.21</sub>Te<sub>0.02</sub>)<sub>Σ4.00</sub>. Zaykovite is monoclinic, space group *C2/m*,  $a = 10.877(1)$ ,  $b = 11.192(1)$ ,  $c = 6.4796(6)$  Å,  $\beta = 108.887(2)^\circ$ ,  $V = 746.3(1)$  Å<sup>3</sup>,  $Z = 6$  and  $D_{\text{calc}} = 8.32$  g cm<sup>-3</sup>. The crystal structure has been solved and refined to  $R_1 = 0.016$  based on 858 unique observed reflections. The strongest lines of the powder X-ray diffraction pattern [ $d(\text{Å})$ , ( $I$ ), ( $hkl$ )] are: 5.43(37)( $\bar{1}11$ ), 3.275(75)(310), 3.199(100)( $\bar{1}31$ ), 3.061(87)(002), 2.568(62)(400), 2.545(41)(041), 3.413(34)( $\bar{2}41$ ) and 1.697(34)(441). Zaykovite is a Se analogue of kingstonite, Rh<sub>3</sub>S<sub>4</sub>. A continuous series of solid solutions between kingstonite and zaykovite was encountered in the samples from the Kazan placer. The possible sources of this unique Rh–Se mineralisation in the South Urals could be serpentinised dunite–harzburgite or gabbro–clinopyroxenite–dunite complexes in the vicinity.

**Keywords:** platinum-group mineral, rhodium, selenide, crystal structure, EBSD, gold placer, South Urals

(Received 15 July 2022; accepted 2 November 2022; Accepted Manuscript published online: 16 November 2022; Associate Editor: František Laufek)

### Introduction

Rhodium and selenium are rare elements with a different geochemical fate and, as a consequence, have a low probability to be combined into rhodium selenide minerals. Platinum-group elements (PGE) are constituents of more than 20 selenides from different localities worldwide (e.g. Johan *et al.*, 1970; Davis *et al.*, 1977; Jebwab *et al.*, 1992; Cook *et al.*, 1994; Polekhovskiy *et al.*, 1997; Paar *et al.*, 1998; Roberts *et al.*, 2002; Vymazalová *et al.*, 2012; Zaykov *et al.*, 2017; Barkov *et al.*, 2017, 2021; Krivovichev, 2021). However, the only natural rhodium selenide reported to date is a poorly defined phase with an inferred formula (Rh,Cu)<sub>9</sub>(Se,S)<sub>11</sub>, described from chromitites of the Luobusa ophiolite deposit, Tibet, China (Bai *et al.*, 2007).

The high abundance of rhodium minerals in the platinum-group mineral (PGM)-bearing gold placers of South Urals, Russia, was established at the end of the last Century, upon the discovery of polkanovite, Rh<sub>12</sub>As<sub>7</sub>, palladodymite, (Pd,Rh)<sub>2</sub>As, and miassite, Rh<sub>17</sub>S<sub>15</sub> (Britvin *et al.*, 1998, 1999, 2001). The PGE mineralogy of ultramafic rocks and placers of

the Uralian Platinum Belt located along the Main Uralian Fault, mainly in the Middle Urals, is well studied (e.g. Stepanov *et al.*, 2019, 2020) (Fig. 1). The Rh-bearing species are represented by minerals of the kashinite–bowieite series and Ir–Rh–Pt thiospinels related to the cuproiridsite–cuprorhodsite–malanite series (Tolstykh *et al.*, 2011, 2015; Malich *et al.*, 2015; Stepanov *et al.*, 2019, 2020; Palamarchuk *et al.*, 2020). Hollingworthite is known as a secondary mineral developed after primary Pt–Fe alloys in the Nizhny Tagil and Kamenushensky massifs (Tolstykh *et al.*, 2011, 2015). Cuprorhodsite occurs among platinum-group minerals of the Nizhny Tagil and the Veresovy Bor massifs (Begizov and Zav'yalov, 2016). Rhodplumsite Rh<sub>3</sub>Pb<sub>2</sub>S<sub>2</sub> and an unnamed telluride (Pb,Bi)Rh<sub>2</sub>Te<sub>3</sub> were described from the Veresovy Bor (Stepanov *et al.*, 2020). However, neither selenide mineralisation nor even selenium impurities in PGM of the primary and placer associations have previously been reported in the deposits belonging to the Uralian Platinum Belt (Stepanov *et al.*, 2020).

The PGE mineralogy of the South Urals is much less studied (Saveliev *et al.*, 2017; Zaykov *et al.*, 2011, 2012, 2017; Zaykova *et al.*, 2020; Rakhimov *et al.*, 2021a, 2021b). Along with Rh minerals from the Miass river placers (Britvin *et al.*, 1998, 1999, 2001), only kashinite with traces of Rh was described in chromitite from the Vladimir deposit of the Varshav ultramafic massif (Ankushev

\*Author for correspondence: Elena V. Belogub, Email: [belogub\\_e@yahoo.com](mailto:belogub_e@yahoo.com)

Cite this article: Belogub E.V., Britvin S.N., Shilovskikh V.V., Pautov L.A., Kotlyarov V.A. and Zaykova E.V. (2023) Zaykovite, Rh<sub>3</sub>Se<sub>4</sub>, a new mineral from the Kazan placer, South Urals, Russia. *Mineralogical Magazine* 87, 118–129. <https://doi.org/10.1180/mgm.2022.122>

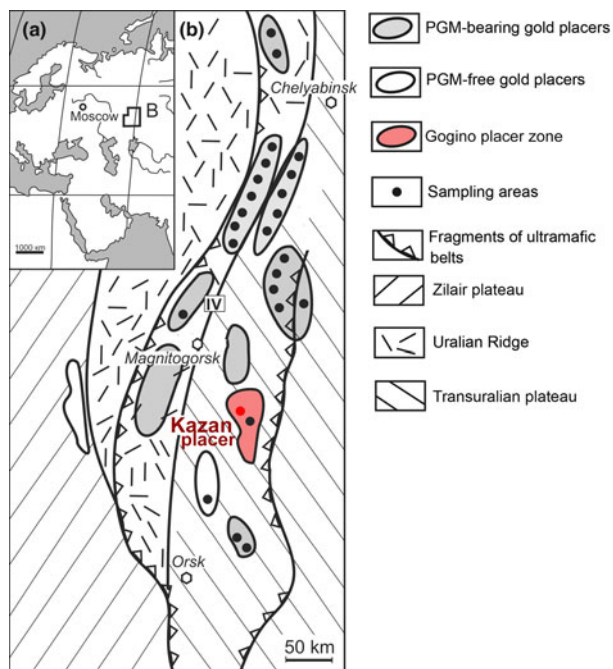


**Fig. 1.** (a) Geographic setting in the South Urals and (b) location of the main placer zones and placers with data on the placer mineral assemblages (simplified after Zaykov *et al.*, 2017). The Gogino placer zone and the Kazan placer within it are marked.

*et al.*, 2016). Selenium-bearing PGM were first discovered by Victor Zaykov (Zaykov *et al.*, 2017) as micro-inclusions of sulfides and sulfoarsenides hosted by native platinum and Ir–Os alloys from the Kazan, Malo-Iremel and Bayramgulov gold placers (the Ingul placer area) (Zaykov *et al.*, 2017; Belogub *et al.*, 2019).

The Kazan placer was found to be most enriched in Se–PGE minerals. In the course of ongoing research on the Kazan PGE assemblages, a new rhodium selenide, ideally  $\text{Rh}_3\text{Se}_4$ , was discovered in this placer. The mineral is named zaykovite, in honour of Victor Vladimirovich Zaykov (1938–2017), Russian geologist and geoarchaeologist, for his contributions to the study of PGE minerals from gold placers of the Urals and other regions (Ankushiev *et al.*, 2016; Zaykov *et al.*, 2017; Artem'ev and Zaykov, 2018). Both the mineral and its name (symbol Zay) have been approved by the Commission on New Minerals, Nomenclature and Classification of the International Mineralogical Association (IMA2019-084, Belogub *et al.*, 2020). Type material is deposited in the collections of the Fersman Mineralogical Museum, Russian Academy of Sciences, Leninskiy Prospekt 18-2, Moscow 119071, Russia, registration number 5395/1.

## Materials and methods

Heavy mineral concentrates enriched with PGM were given to Victor Zaykov by A.Yu. Ivanov and B.Ya. Hismatullin (OOO (limited company) “Miasskiy priisk”). The sample was collected in open pit No.3 of the Kazan placer in July, 2017.

The chemical composition of zaykovite was determined using an Oxford link REMMA 2M scanning electron microscope (SEM) with energy-dispersive spectroscopy (EDS). Operating conditions were: acceleration voltage = 20 kV, beam current = 6 nA and beam diameter = 2  $\mu\text{m}$ . Reference materials were metallic Rh, Pt, Os, Ir, Ru, Pd, Au, Ag for respective metals, chalcopyrite (for S, Fe and

Cu), CdSe and  $\text{Bi}_2\text{Se}_3$  (for Se) using the NERMA.GEOL.25.10.74, Kyiv, 2005 standards at the South Urals Federal Research Center of Mineralogy and Geoecology. Electron microprobe analysis was done using a JEOL JXA-733 with a wavelength dispersive spectrometer (WDS) at the Fersman Mineralogical Museum using an acceleration voltage of 20 kV, a beam current of 20 nA and a beam diameter of 2  $\mu\text{m}$ . Reference materials were metallic Rh, Pt, Ir, Ru, Pd for respective metals, pyrite (for S and Fe),  $\text{Bi}_2\text{Se}_3$  (for Se) and HgTe (for Te).

The formulae were calculated for 7 atoms per formula unit for the kingstonite–zaykovite series minerals, 15 atoms for the Pd–Sb–Te phase, and 1 atom for the Pt–Fe and Au–Pd alloys.

Element-distribution maps and additional data on composition were obtained at the Geomodel Resource Center (Saint Petersburg State University (SPbU), St Petersburg, Russia) on a Hitachi S-3400N SEM equipped with an Oxford Instruments X-Max 20 EDA at an accelerating voltage of 10 kV and a beam current of 1 nA spatial resolution. The spectrometer was calibrated against a set of standard natural and synthetic samples, (Micro-Analysis Consultants Ltd (MAC) standards).

The electron back-scattered diffraction (EBSD) maps were obtained using an Oxford Instruments HKL NordlysNano detector (Geomodel Resource Center, Scientific Park, SPbU) mounted on the abovementioned SEM. The acquisition conditions were as follows: 30 kV and 1.5 nA, an exposition of 0.5 s per pattern, averaging 5–10 images (when mapping) or 20 images (to obtain individual patterns), and their subsequent processing using the *Channel5* software package from Oxford Instruments. Kingstonite crystal structure data (AMCSD<sup>1</sup> № 0014575) was used for the comparison, isoferroplatinum (ICSD<sup>2</sup> 56275), platinum (ICSD 76153) and mertieite-II (Karimova *et al.*, 2018) structure data were used as references for EBSD mapping.

Data on the orientation of the individual crystals of zaykovite are shown in Euler colour schemes, pole figures and orientation distribution density heatmaps (Mason and Schuh, 2009).

To obtain a mechanically undistorted surface, the sample for EBSD analysis was treated with a direct beam of Ar plasma using an Oxford Instruments Ionfab300 etcher, an exposition of 10 min, an angle of 45, an accelerating voltage of 500 V, a current of 200 mA and a beam diameter of 10 cm (Nanophotonics Resource Center, Scientific Park, SPbU).

Reflectance data for zaykovite were obtained using a microscope-spectrophotometer LOMO MSP-R equipped with a spectrophotometric attachment PEI “R928” (Hamamatsu, Japan) at the South Urals Federal Research Center of Mineralogy and Geoecology, Miass, Russia. The measurements were done in air using a  $\times 40$  objective with a 0.65 numerical aperture: a photometric diaphragm of 0.3 mm; an analysing area of  $0.007 \times 0.007$  mm; a diffraction grating of 600 grooves/mm; a spectral interval of 6 nm; a voltage of 450 V and elemental silicon as a standard. The measurements were provided for the 400–700 nm range.

The zaykovite grain used for the single-crystal study was extracted from the Pt–Fe alloy matrix manually, by gentle indentation of the adjacent metal with a tungsten carbide needle. Single-crystal data were collected by means of a Bruker Kappa APEX DUO CCD diffractometer using  $\text{MoK}\alpha$  radiation. Data collection and integration procedures were performed using Bruker APEX2 and Bruker SAINT software (Bruker Inc., Wisconsin,

<sup>1</sup>American Mineralogist Crystal Structure Database, <http://ruff.geo.arizona.edu/AMS/amcsd.php>

<sup>2</sup>Inorganic Crystal Structure Database, <https://www.pds.ac.uk/icsd>

USA). The crystal structure of zaykovite was solved using the dual space method and refined to  $R_1 = 0.0158$  with the *SHELX*-2014 set of programs (Sheldrick, 2015) via *Olex2* v.1.2.8 graphical user interface (Dolomanov *et al.*, 2009). For mixed site occupancies, we used scattering factors of neutral atoms for Rh and Pt (sites M1–M4) and Se and S (sites X1–X4). Data collection and structure refinement details can be retrieved from the crystallographic information file (CIF) deposited with the Principal Editor of *Mineralogical Magazine* and available as Supplementary material (see below).

Powder X-ray diffraction data were obtained using a Rigaku R-Axis Rapid II diffractometer with a curved (cylindrical) imaging plate detector ( $r = 127.4$  mm). Conditions were:  $\text{CoK}\alpha$  radiation ( $\lambda = 1.79021$  Å), rotating anode (40 kV, 15 mA) with microfocus optics and a Gandolfi method with an exposure time of 60 min. The image-to-profile data conversion was completed using the *osc2xrd* program (Britvin *et al.*, 2017). The theoretical pattern was calculated on the basis of atomic coordinates obtained from the structure refinement and unit-cell parameters refined from the powder diffraction data, by means of *WinXPOW* software (Stoe & Cie GmbH, Darmstadt, Germany). Calculated lines having the intensity  $< 2$  have been omitted.

### Geological background for the Kazan gold placer

Zaykovite was found in a heavy mineral concentrate obtained from the Kazan gold-bearing placer, which is a part of the

Gogino placer zone (Zaykov *et al.*, 2017),  $52^\circ 42' 00''\text{N}$ ,  $60^\circ 26' 27''\text{E}$ , located 100–150 km to the SSE from the city of Magnitogorsk in the Chelyabinsk region, Russia (Fig. 1) and includes ~20 placers, represented by the Mesozoic and Miocene karst and eluvial placers, 1.0–3.0 km long and 80–200 m wide. The most productive karst placers produced more than 2 t of gold during the period 1851–2004 with 925–901‰ fineness (Ivanishchev *et al.*, 2005). Native gold grains are mostly small and poorly rounded, which indicates proximity to the source (Zaykov *et al.*, 2017).

The Kazan placer is in the Bredy erosion-structural depression of Cenomanian–Upper Pleistocene age (Fig. 2a). It is located at the confluence of the Karagayly-Ayat and Kamyshly-Ayat rivers. The length of the placer exceeds 4 km with a highly variable width and a complex nesting stream-like morphology. There are no permanent watercourses in close proximity to the placer. The thickness of peat is from 1.5 to 35 m, sands from 0.2 to 4.3 m. The underlying rock is represented by karst Lower Carboniferous limestone (Fig. 2b). The Varshavka and Gogino ultramafic massifs are the nearest potential sources for platinum-group minerals (PGM) in the placer.

The placer was exploited during 1851–1910. In 1996, exploitation was restarted (unpublished report of the Geological Survey of Chelyabinsk Geological Committee).

It was previously established that the heavy mineral concentrate of the Kazan placer mainly consists of chromite, platinum

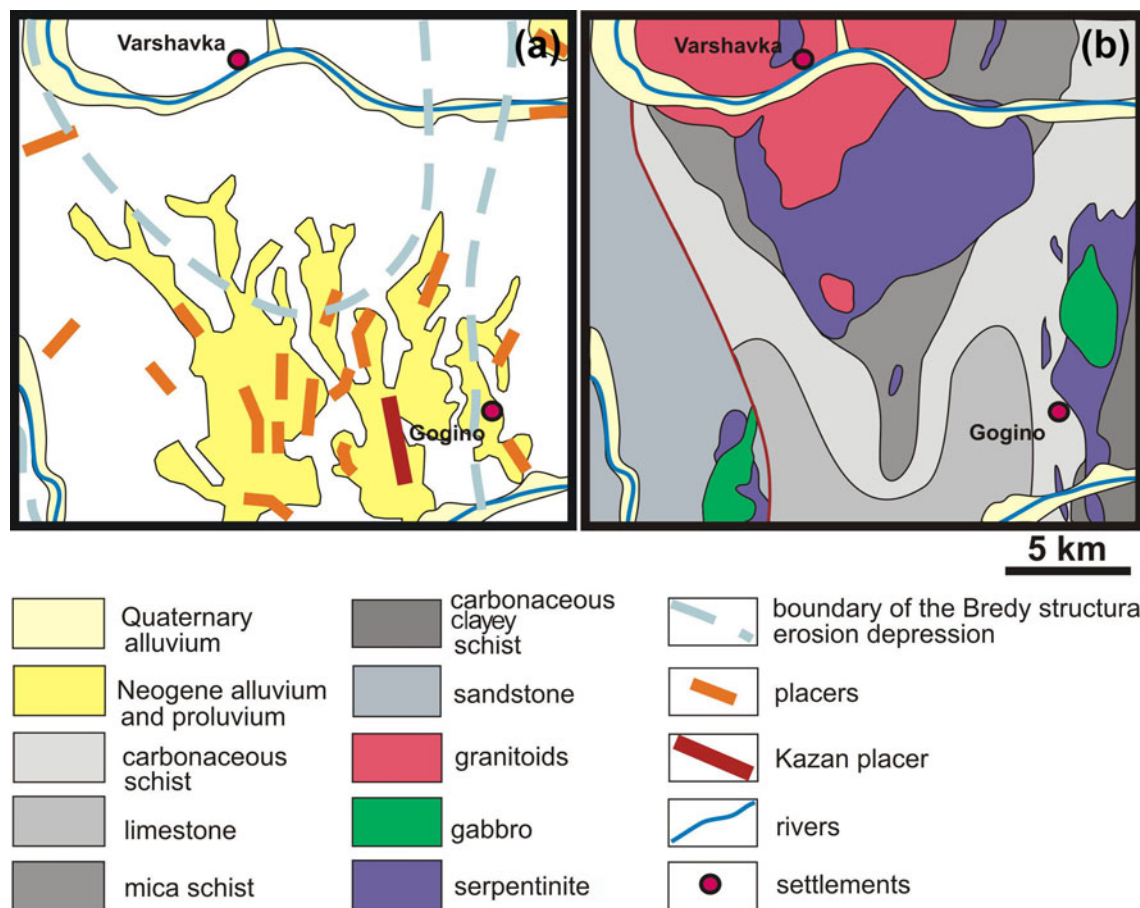


**Fig. 2.** (a) Position of the Kazan placer on the geological map of the Gogino placer zone within the Bredy structural erosion depression and (b) geological map of the underlying Palaeozoic basement.

**Table 1.** Chemical composition of a Pt–Fe alloy grain with zaykovite inclusions (wt.%, EDS).

No	Os	Fe	Pt	Cu	Total	Calculated formulae
1	0.49	6.69	92.19	0.45	99.82	Pt <sub>0.78</sub> Fe <sub>0.20</sub> Cu <sub>0.01</sub>
2	–	6.21	93.13	0.71	100.07	Pt <sub>0.80</sub> Fe <sub>0.18</sub> Cu <sub>0.02</sub>
3	–	6.75	92.69	0.34	99.81	Pt <sub>0.78</sub> Fe <sub>0.20</sub> Cu <sub>0.01</sub>

Notes. Dash – below limit of detection

**Table 2.** Chemical composition of the Au–Pd alloy (wt.%, EDS).

	Pd	Au	Cu	Pt	Ag	total	Calculated formulae
1	8.23	87.04	1.59	2.61	0.43	99.9	Au <sub>0.79</sub> Pd <sub>0.14</sub> Cu <sub>0.04</sub> Pt <sub>0.02</sub> Ag <sub>0.01</sub>
2	8.34	85.86	1.34	3.76	0.57	99.87	Au <sub>0.78</sub> Pd <sub>0.14</sub> Cu <sub>0.04</sub> Pt <sub>0.03</sub> Ag <sub>0.01</sub>
3	7.55	84.75	1.47	5.06	0.81	99.64	Au <sub>0.77</sub> Pd <sub>0.13</sub> Cu <sub>0.05</sub> Pt <sub>0.03</sub> Ag <sub>0.01</sub>
4	9.12	85.90	1.34	2.88	0.43	99.67	Au <sub>0.78</sub> Pd <sub>0.15</sub> Cu <sub>0.04</sub> Pt <sub>0.03</sub> Ag <sub>0.01</sub>

alloy (min-max-mean, wt.%): Pt 76–93–90.3, Fe 2.6–9.8–7.4, Cu 0.2–4.0 and gold alloy with a fineness of 780–1000, mean ~890–900 (Zaykova *et al.*, 2020). Pt–Fe alloy grains constitute up to 73% of all PGM in the heavy-mineral concentrate. Native

**Table 3.** Chemical composition of the Pd–Sb–Te phase (wt.%, EDS).

Nº	Pd	Pt	Ag	Sb	Te	As	Total	Calculated formulae
1	64.09	7.7	–	18.92	9.06	–	99.77	(Pd <sub>10.41</sub> Pt <sub>0.68</sub> )Σ11.09(Sb <sub>2.68</sub> Te <sub>1.23</sub> )Σ3.91
2	63.72	7.93	–	18.81	9.44	–	99.89	(Pd <sub>10.35</sub> Pt <sub>0.70</sub> )Σ11.05(Sb <sub>2.67</sub> Te <sub>1.28</sub> )Σ3.95
3	62.88	7.96	1.02	19.35	8.34	–	99.54	(Pd <sub>10.24</sub> Pt <sub>0.71</sub> Ag <sub>0.16</sub> )Σ11.11(Sb <sub>2.75</sub> Te <sub>1.13</sub> )Σ3.88
4	61.96	7.98	–	14.11	15.84	–	99.89	(Pd <sub>10.12</sub> Pt <sub>0.71</sub> )Σ10.83(Te <sub>2.16</sub> Sb <sub>2.01</sub> )Σ4.17
5	61.01	10.35	–	20.25	7.91	–	99.52	(Pd <sub>10.06</sub> Pt <sub>0.93</sub> )Σ10.99(Sb <sub>2.92</sub> Te <sub>1.09</sub> )Σ4.01
6	61.28	9.7	–	19.63	9.01	–	99.62	(Pd <sub>10.07</sub> Pt <sub>0.87</sub> )Σ10.94(Sb <sub>2.82</sub> Te <sub>1.24</sub> )Σ4.06
7	61.76	8.22	1.6	18.35	9.56	0.43	99.9	(Pd <sub>10.02</sub> Pt <sub>0.73</sub> Ag <sub>0.26</sub> )Σ11.01(Sb <sub>2.60</sub> Te <sub>1.29</sub> As <sub>0.10</sub> )Σ3.99
8	53.91	19.17	1.11	19.75	5.77	–	99.7	(Pd <sub>9.24</sub> Pt <sub>1.79</sub> Ag <sub>0.19</sub> )Σ11.22(Sb <sub>2.60</sub> Te <sub>1.29</sub> )Σ3.89
9	59.79	13.31	–	18.42	7.91	–	99.43	(Pd <sub>9.99</sub> Pt <sub>1.21</sub> )Σ11.20(Sb <sub>2.69</sub> Te <sub>1.10</sub> )Σ3.79

Notes. Dash – below limit of detection.

**Table 4.** Reflectance values measured in air versus Si reference standard.

$R_{max}$	$R_{min}$	$\lambda$ (nm)	$R_{max}$	$R_{min}$	$\lambda$ (nm)
29.4	28.8	400	32.5	31.3	560
29.5	28.9	420	33.1	31.8	580
29.5	29.1	440	<b>33.4</b>	<b>32.0</b>	<b>589</b>
29.9	29.3	460	33.7	32.3	600
<b>30.1</b>	<b>29.3</b>	<b>470</b>	34.3	32.9	620
30.2	29.4	480	34.8	33.5	640
30.7	29.7	500	<b>35.1</b>	<b>33.7</b>	<b>650</b>
31.3	30.2	520	35.3	34.0	660
31.9	30.7	540	35.8	34.6	680
<b>32.2</b>	<b>31.0</b>	<b>546</b>	36.3	35.1	700

The reference wavelengths required by the Commission on Ore Mineralogy (COM) are given in bold.

metals (gold alloys and alloys of the system Os–Ir–Ru, laurite–erlichmanite, sulfarsenides (irarsite, hollingworthite), stibiopalladinite and some unnamed phases enriched with Rh, Ru and Se form inclusions within grains of Pt–Fe alloys (Zaykova *et al.*, 2020).

The grains of Pt–Fe alloys are angular with relics of growth sculpture and imprints of other minerals, probably indicating

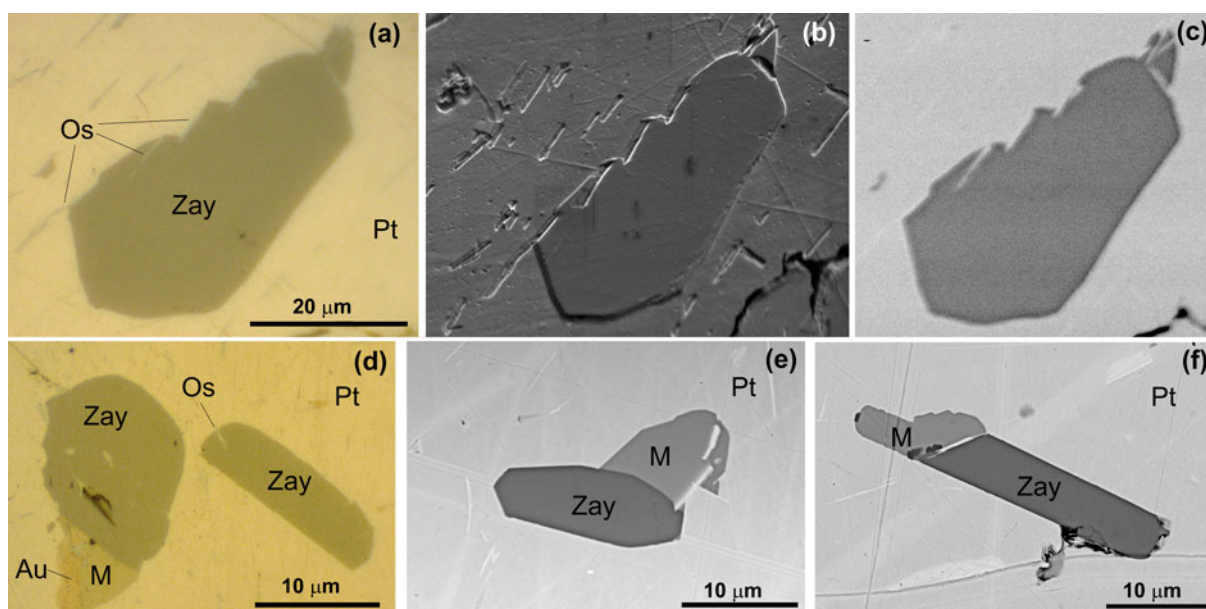


**Fig. 3.** Morphology of zaykovite (Zay) inclusions in the Pt–Fe alloy (Pt). (a–c) Holotype zaykovite (5395/1), single crystal with thin osmium lamellae (Os); (d) intergrowth with Pd–Sb–Te phase (M) and Pd-rich gold (Au); (e, f) intergrowth with a Pd–Sb–Te phase (M). (a, d) Photo in reflected light (oil immersion); (b) SE image tilted to 70° of the same area, after argon plasma etching; and (c, e, f) back-scattered electron (BSE) images.

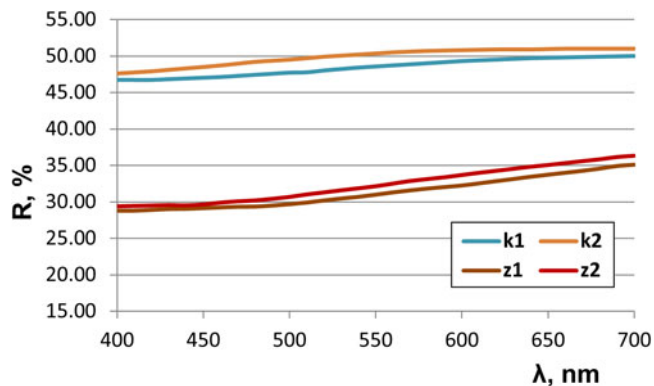


**Fig. 4.** Reflection spectra of zaykovite (z1 and z2) in comparison with kingstonite (k1 and k2) (Stanley *et al.*, 2005).

short distances from their primary source (Zaykova *et al.*, 2020). Laser ablation inductively-coupled plasma mass spectrometry (LA-ICP-MS) analysis of 5 grains of Pt–Fe alloy from the Kazan placer showed elevated contents of (ppm, mean) As (113), Sb (845), Au (2455), Hg (150), Rh (4640), Pd (460), Os (6890), Ir (6890), Te (1.9), Ag (2.2), Mo (4.2) and elements characteristic of chromite (Cr, Mn and V). Selenium contents were below the limit of detection of ~1 ppm (Artem'ev and Zaykov, 2018).

**Results**

**Morphology, association and physical properties**

The heavy concentrate studied consisted of chromite, platinum and gold alloys. Fe–Pt alloy grains with zaykovite inclusions are ~1 mm in size and contain some Cu (Table 1). According to EBSD data the Pt–Fe alloys have a good conformity with isoferroplatinum (ICSD 56275) with mean angle deviation (MAD) of 0.20–0.28° and with platinum (ICSD 76153) with MAD of 0.23–0.4°. The EBSD patterns of isoferroplatinum and platinum are very similar and can not be reliably distinguished purely on EBSD basis, thus we use ‘Pt–Fe alloys’ as the mineral name according to Cabri and Feather (1975) and Cabri *et al.* (2022). Micrometre-size inclusions of Au–Pd alloy (Table 2) and the Pd–Sb–Te phase (Table 3, Supplementary material C) occur within the grain hosting the zaykovite studied. According to EBSD the structure of Pd–Sb–Te phase is close to mertieite-II with the MAD of 0.48°.

Zaykovite was found as elongated idiomorphic crystals up to 40 μm in size (Fig. 3). Zaykovite forms intergrowths with a Pd–Sb–Te phase (Fig. 3d–f) and Au–Pd alloy (Fig. 3d).

Under reflected light, zaykovite is grey with a bluish-greenish tint in comparison with the Pt–Fe alloy. It has a yellow-greenish tint in oil immersion (Figs 3a, d). Zaykovite has a metallic lustre and black streak. Polarised light reveals its weak birefractance and

**Table 5.** Chemical composition of the zaykovite holotype (1–5, WDS) and minerals of kingstonite–zaykovite series from the Kazan placer (6–18, EDS) (wt.%).

	Os	Ir	Ru	Rh	Pt	Pd	Fe	S	Se	Te	Total
1	–	7.72	0.20	36.46	14.60	0.18	0.04	6.02	34.92	0.50	100.63
2	–	7.33	0.27	36.74	14.43	0.12	0.05	6.24	35.01	0.46	100.66
3	–	7.70	0.19	36.76	14.92	0.14	0.04	6.24	34.16	0.44	100.58
4	–	7.47	0.22	37.22	14.04	0.08	0.10	6.26	34.90	0.50	100.77
5	–	8.61	0.16	37.32	13.32	0.16	0.05	5.98	34.31	0.33	100.24
mean	–	7.77	0.21	36.90	14.26	0.14	0.06	6.15	34.66	0.45	100.58
6	2.59	5.48	0.40	35.49	8.19	–	0.37	2.17	32.07	13.25	100.00
7	0.21	3.98	0.31	41.53	3.05	0.54	0.14	–	48.85	0.45	96.06
8	–	7.40	–	44.13	1.94	–	–	4.34	42.25	0.83	100.90
9	–	4.16	–	47.28	14.10	–	–	15.25	19.22	–	100.00
10	0.36	0.89	0.47	48.65	12.08	0.61	0.36	12.27	24.29	–	100.00
11	–	12.04	–	36.18	14.23	0.22	–	11.23	25.39	–	99.29
12	–	0.46	0.35	53.44	8.50	–	–	14.57	23.12	–	100.43
13	–	–	0.35	52.26	8.68	–	–	14.65	23.86	0.34	100.13
4	–	7.64	–	52.23	12.52	0.68	0.11	26.64	1.06	–	100.89
15	–	5.19	1.15	55.65	9.58	–	–	24.45	4.10	–	100.11
16	–	7.20	–	58.34	3.94	–	0.24	29.26	1.71	–	100.69

Calculated formulae (7 apfu)

1	(Rh <sub>2.24</sub> Pt <sub>0.47</sub> Ir <sub>0.25</sub> Ru <sub>0.01</sub> Pd <sub>0.01</sub> Fe <sub>0.01</sub> )Σ <sub>2.99</sub> (Se <sub>2.79</sub> S <sub>1.19</sub> Te <sub>0.02</sub> )Σ <sub>4.01</sub>
2	(Rh <sub>2.24</sub> Pt <sub>0.46</sub> Ir <sub>0.24</sub> Ru <sub>0.02</sub> Pd <sub>0.01</sub> Fe <sub>0.01</sub> )Σ <sub>2.97</sub> (Se <sub>2.78</sub> S <sub>1.22</sub> Te <sub>0.02</sub> )Σ <sub>4.03</sub>
3	(Rh <sub>2.26</sub> Pt <sub>0.48</sub> Ir <sub>0.25</sub> Ru <sub>0.01</sub> Pd <sub>0.01</sub> )Σ <sub>3.02</sub> (Se <sub>2.73</sub> S <sub>1.23</sub> Te <sub>0.02</sub> )Σ <sub>3.98</sub>
4	(Rh <sub>2.26</sub> Pt <sub>0.45</sub> Ir <sub>0.24</sub> Ru <sub>0.01</sub> Fe <sub>0.01</sub> )Σ <sub>2.99</sub> (Se <sub>2.77</sub> S <sub>1.22</sub> Te <sub>0.02</sub> )Σ <sub>4.01</sub>
5	(Rh <sub>2.30</sub> Pt <sub>0.43</sub> Ir <sub>0.28</sub> Ru <sub>0.01</sub> Pd <sub>0.01</sub> Fe <sub>0.01</sub> )Σ <sub>3.04</sub> (Se <sub>2.76</sub> S <sub>1.18</sub> Te <sub>0.02</sub> )Σ <sub>3.96</sub>
mean	(Rh <sub>2.26</sub> Pt <sub>0.46</sub> Ir <sub>0.25</sub> Ru <sub>0.01</sub> Pd <sub>0.01</sub> Fe <sub>0.01</sub> )Σ <sub>3.00</sub> (Se <sub>2.77</sub> S <sub>1.21</sub> Te <sub>0.02</sub> )Σ <sub>4.00</sub>
6	(Rh <sub>2.37</sub> Pt <sub>0.29</sub> Ir <sub>0.38</sub> Ru <sub>0.03</sub> Fe <sub>0.05</sub> )Σ <sub>3.02</sub> (Se <sub>2.79</sub> S <sub>0.47</sub> Te <sub>0.71</sub> )Σ <sub>3.98</sub>
7	(Rh <sub>2.63</sub> Ir <sub>0.13</sub> Pt <sub>0.10</sub> Pd <sub>0.03</sub> Ru <sub>0.02</sub> Fe <sub>0.02</sub> )Σ <sub>2.95</sub> (Se <sub>4.03</sub> Te <sub>0.02</sub> )Σ <sub>4.05</sub>
8	(Rh <sub>2.60</sub> Ir <sub>0.23</sub> Pt <sub>0.06</sub> )Σ <sub>2.89</sub> (Se <sub>3.25</sub> S <sub>0.82</sub> Te <sub>0.04</sub> )Σ <sub>4.11</sub>
9	(Rh <sub>2.53</sub> Pt <sub>0.40</sub> Ir <sub>0.12</sub> )Σ <sub>3.04</sub> (Se <sub>2.77</sub> S <sub>1.21</sub> Te <sub>0.02</sub> )Σ <sub>3.96</sub>
10	(Rh <sub>2.65</sub> Pt <sub>0.35</sub> Ir <sub>0.03</sub> Ru <sub>0.03</sub> Fe <sub>0.04</sub> Pd <sub>0.03</sub> )Σ <sub>3.13</sub> (Se <sub>2.77</sub> S <sub>1.21</sub> Te <sub>0.02</sub> )Σ <sub>3.87</sub>
11	(Rh <sub>2.12</sub> Pt <sub>0.44</sub> Ir <sub>0.38</sub> Pd <sub>0.01</sub> )Σ <sub>2.95</sub> (S <sub>2.11</sub> Se <sub>1.94</sub> )Σ <sub>4.05</sub>
12	(Rh <sub>2.76</sub> Pt <sub>0.23</sub> Ru <sub>0.02</sub> Ir <sub>0.01</sub> )Σ <sub>3.03</sub> (S <sub>2.42</sub> Se <sub>1.56</sub> )Σ <sub>3.97</sub>
13	(Rh <sub>2.70</sub> Pt <sub>0.24</sub> Ru <sub>0.01</sub> )Σ <sub>2.95</sub> (S <sub>2.43</sub> Se <sub>1.61</sub> Te <sub>0.01</sub> )Σ <sub>4.05</sub>
14	(Rh <sub>2.43</sub> Pt <sub>0.31</sub> Ir <sub>0.19</sub> Pd <sub>0.03</sub> Fe <sub>0.01</sub> )Σ <sub>2.96</sub> (S <sub>2.96</sub> Se <sub>0.06</sub> )Σ <sub>4.00</sub>
15	(Rh <sub>2.62</sub> Pt <sub>0.24</sub> Ir <sub>0.13</sub> Ru <sub>0.06</sub> )Σ <sub>3.05</sub> (S <sub>3.70</sub> Se <sub>0.25</sub> )Σ <sub>3.95</sub>
16	(Rh <sub>2.54</sub> Pt <sub>0.09</sub> Ir <sub>0.17</sub> Fe <sub>0.02</sub> )Σ <sub>2.82</sub> (S <sub>4.08</sub> Se <sub>0.10</sub> )Σ <sub>4.18</sub>

Note. 1–5 – (WDA of holotype), 6–16 EDA. Dash, As, Sb – below limit of detection.

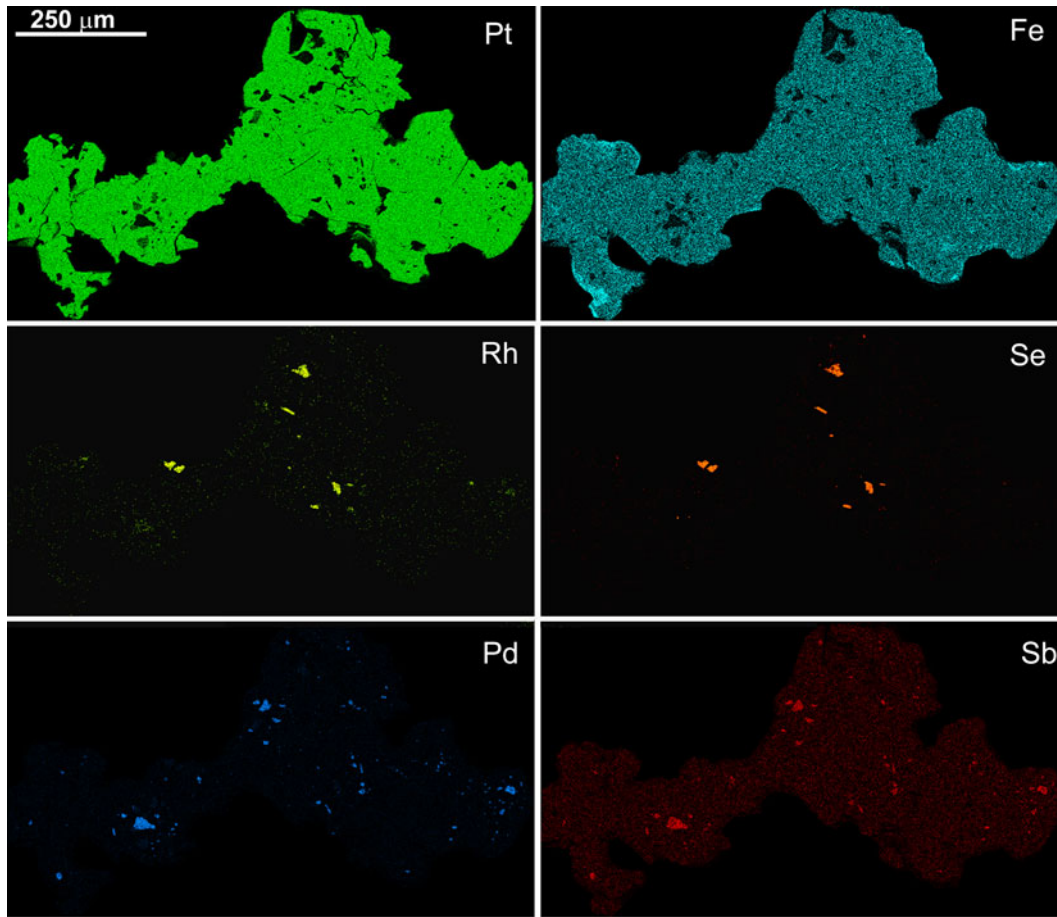


Fig. 5. Elemental distribution EDS maps of Pt-Fe alloy with zaykovite and Pd-Sb-Te phase inclusions.

Table 6. Powder X-ray diffraction data (*d* in Å) for zaykovite.\*

<i>I</i> <sub>meas</sub>	<i>d</i> <sub>meas</sub>	<i>I</i> <sub>calc</sub>	<i>d</i> <sub>calc</sub>	<i>hkl</i>	<i>I</i> <sub>meas</sub>	<i>d</i> <sub>meas</sub>	<i>I</i> <sub>calc</sub>	<i>d</i> <sub>calc</sub>	<i>hkl</i>
		5	7.562	110			4	1.928	$\bar{4}$ 03
<b>37</b>	<b>5.43</b>	3	5.593	020			3	1.886	$\bar{3}$ 51
		<b>15</b>	<b>5.428</b>	<b><math>\bar{1}</math>11</b>			6	1.872	350
		16	5.131	200	20	1.861	29	1.864	060
		4	4.759	$\bar{2}$ 01			6	1.861	113
		2	4.284	111	22	1.855	43	1.853	$\bar{1}$ 33
		2	4.128	021			8	1.839	$\bar{1}$ 52
		2	3.781	220			6	1.822	423
		9	3.624	$\bar{2}$ 21			3	1.812	442
<b>75</b>	<b>3.275</b>	5	3.425	201			4	1.805	$\bar{6}$ 01
<b>100</b>	<b>3.199</b>	<b>57</b>	<b>3.271</b>	<b>310</b>	12	1.787	15	1.786	532
		<b>100</b>	<b>3.196</b>	<b><math>\bar{1}</math>31</b>			4	1.785	242
		8	3.104	$\bar{2}$ 02	16	1.754	17	1.753	$\bar{6}$ 02
<b>87</b>	<b>3.061</b>	<b>64</b>	<b>3.059</b>	<b>002</b>			3	1.752	260
		10	2.921	221			6	1.752	332
		2	2.906	131	8	1.740	4	1.739	352
28	2.700	14	2.696	401			7	1.736	513
		14	2.685	312	9	1.714	11	1.715	203
19	2.630	6	2.627	112			2	1.713	402
<b>62</b>	<b>2.568</b>	<b>43</b>	<b>2.566</b>	<b>400</b>			6	1.710	600
		29	2.554	331			7	1.708	351
<b>41</b>	<b>2.545</b>	<b>42</b>	<b>2.543</b>	<b>041</b>			10	1.703	243
		6	2.521	330	<b>34</b>	<b>1.697</b>	<b>43</b>	<b>1.696</b>	<b>441</b>
31	2.438	13	2.441	$\bar{1}$ 32			3	1.684	133

(Continued)

Table 6. (Continued.)

<i>I</i> <sub>meas</sub>	<i>d</i> <sub>meas</sub>	<i>I</i> <sub>calc</sub>	<i>d</i> <sub>calc</sub>	<i>hkl</i>	<i>I</i> <sub>meas</sub>	<i>d</i> <sub>meas</sub>	<i>I</i> <sub>calc</sub>	<i>d</i> <sub>calc</sub>	<i>hkl</i>
		14	2.429	421			2	1.615	$\bar{2}$ 04
<b>34</b>	<b>2.413</b>	<b>18</b>	<b>2.411</b>	<b>241</b>	7	1.607	7	1.607	531
27	2.321	16	2.319	202			9	1.592	062
		4	2.166	241	13	1.591	4	1.590	533
		2	2.157	331			4	1.587	443
22	2.150	12	2.148	$\bar{2}$ 03			4	1.586	$\bar{6}$ 03
20	2.131	10	2.129	511			6	1.552	404
		3	2.105	$\bar{1}$ 51			2	1.547	$\bar{1}$ 71
20	2.100	13	2.098	113			3	1.533	461
20	2.076	18	2.078	242			3	1.532	313
		4	2.064	042			4	1.508	460
		4	2.035	313			2	1.505	552
		5	2.019	510			5	1.485	642
		6	2.015	151			5	1.463	514
23	2.007	10	2.005	223			5	1.453	262
		5	2.002	512			3	1.448	370
		14	1.993	421			3	1.442	153
22	1.955	23	1.954	312			2	1.432	$\bar{1}$ 72
33	1.943	38	1.941	441			2	1.428	333

\*The strongest lines are given in bold.

anisotropy, but no internal reflexions. Reflectance values are shown in Table 4. Zaykovite has significantly lower reflectance than kingstonite (Fig. 4).

Zaykovite is slightly harder than the Pt-Fe alloy and softer than native osmium. Mohs hardness is estimated as 5½. Micro-

**Table 7.** Crystal parameters, data collection and structure refinement details for zaykovite.

Crystal data	
Formula*	(Rh <sub>2.43</sub> Pt <sub>0.57</sub> )Σ <sub>3.00</sub> (Se <sub>2.85</sub> S <sub>1.16</sub> )Σ <sub>4.00</sub>
Crystal size (mm)	0.03 × 0.02 × 0.02
Crystal system	Monoclinic
Space group	C2/m
<i>a</i> (Å)	10.877(1)
<i>b</i> (Å)	11.192(1)
<i>c</i> (Å)	6.4796(6)
β (°)	108.887(2)
<i>V</i> (Å <sup>3</sup> )	746.33(12)
<i>Z</i>	6
<i>D<sub>x</sub></i> (g cm <sup>-3</sup> )	8.318
Data collection and refinement	
Radiation	MoKα (λ = 0.71073 Å)
Temperature (K)	293
2θ range (°)	4.00–54.00
Total reflections collected	3263
No. unique reflections	858
No. unique observed, <i>I</i> ≥ 2σ( <i>I</i> )	804
<i>h</i> , <i>k</i> , <i>l</i> range	–13→13, –14→14, –8→8
<i>F</i> (000)	1614
μ (mm <sup>-1</sup> )	45.11
No. refined parameters	63
<i>R</i> <sub>int</sub>	0.024
<i>R</i> <sub>1</sub> [ <i>F</i> ≥ 4σ( <i>F</i> )]	0.016
<i>wR</i> <sub>2</sub>	0.037
<i>S</i> = <i>Gof</i>	1.050
Residuals (e <sup>-</sup> Å <sup>-3</sup> ) (min, max)	–1.29, 0.93
Data completeness	1.000

\*Determined via site occupancy refinement.

indentation could not be measured because of the small size of all grains excluding the holotype which was preserved for the museum collection. Cleavage was not observed. When preparing a microsample for single-crystal diffractometry, brittle tenacity was observed. Density was calculated on the basis of structural formula and unit cell parameters, and refined from single-crystal data resulting in a value of 8.318 g·cm<sup>-3</sup>. Because of the small grain size the density was not measured directly. Zaykovite is non-magnetic.

### Chemical composition

The chemical composition of the zaykovite is shown in Table 5. The empirical formula calculated on the basis of 7 atoms per formula unit is (Rh<sub>2.26</sub>Pt<sub>0.46</sub>Ir<sub>0.25</sub>Ru<sub>0.01</sub>Pd<sub>0.01</sub>Fe<sub>0.01</sub>)Σ<sub>3.00</sub>(Se<sub>2.77</sub>S<sub>1.21</sub>Te<sub>0.02</sub>)Σ<sub>4.00</sub>. The simplified formula is (Rh,Pt,Ir)<sub>3</sub>(Se,S)<sub>4</sub>. The ideal formula is Rh<sub>3</sub>Se<sub>4</sub>, which requires (wt.%): Rh 49.44 and Se 50.56.

The distribution of the main elements in the Pt–Fe alloy grain studied shows that zaykovite is the only compound with Rh and Se (Fig. 5).

**Table 8.** Fractional atomic coordinates and isotropic displacement parameters (Å<sup>2</sup>) for zaykovite.

Site*	Occupancy	<i>x</i>	<i>y</i>	<i>z</i>	<i>U</i> <sub>iso</sub>
M1 (8j)	Rh <sub>0.71</sub> Pt <sub>0.29</sub>	0.36923(2)	0.14068(3)	0.44995(4)	0.00817(13)
M2 (4i)	Rh <sub>0.96</sub> Pt <sub>0.04</sub>	0.35205(4)	0	0.05982(8)	0.0086(2)
M3 (2d)	Rh <sub>0.87</sub> Pt <sub>0.13</sub>	0	0	½	0.0072(2)
M4 (4h)	Rh <sub>0.83</sub> Pt <sub>0.17</sub>	0	0.16106(4)	0	0.00706(18)
X1 (4i)	Se <sub>0.64</sub> S <sub>0.36</sub>	0.41600(7)	0	0.73608(13)	0.0089(3)
X2 (8j)	Se <sub>0.94</sub> S <sub>0.06</sub>	0.12949(4)	0.15737(4)	0.39186(7)	0.00745(16)
X3 (4i)	Se <sub>0.66</sub> S <sub>0.34</sub>	0.11709(7)	0	0.89312(13)	0.0074(3)
X4 (8j)	Se <sub>0.55</sub> S <sub>0.45</sub>	0.35468(5)	0.20880(6)	0.09986(9)	0.0085(2)

\*Site multiplicities and Wyckoff symbols are given in parentheses.

**Table 9.** Selected bond lengths (Å) for zaykovite and kingstonite.

Bond	Zaykovite	Kingstonite*
Rh1–X1**	2.3589(7)	2.278(4)
Rh1–X2	2.5181(5)	2.366(4)
Rh1–X2	2.4799(6)	2.406(4)
Rh1–X4	2.3494(7)	2.285(4)
<Rh1–X>	2.427	2.334
Rh1–Rh1	2.7054(6)	2.674(2)
Rh1–Rh2	2.9323(6)	2.875(2)
Rh2–X1	2.4401(9)	2.365(6)
Rh2–X1	2.4144(10)	2.326(6)
Rh2–X3	2.4312(9)	2.324(6)
Rh2–X4	2.3504(7) × 2	2.278(4) × 2
<Rh2–X>	2.397	2.314
Rh3–X2	2.4932(5) × 4	2.390(4) × 4
Rh3–X3	2.4516(8) × 2	2.355(6) × 2
<Rh3–X>	2.479	2.378
Rh4–X2	2.4733(5) × 2	2.357(4) × 2
Rh4–X3	2.4335(6) × 2	2.337(4) × 2
Rh4–X4	2.3876(7) × 2	2.320(4) × 2
<Rh4–X>	2.431	2.338
X4–X4	2.4089(11)	2.237(8)

\*Stanley *et al.* (2005) \*\*X = Se (zaykovite), S (kingstonite).

### Crystal structure and powder X-ray diffraction

Zaykovite crystallises in the monoclinic system in space group *C2/m* (#12). Unit-cell parameters refined from the single-crystal X-ray data are: *a* = 10.8769(11), *b* = 11.1921(11), *c* = 6.4796(6) Å, β = 108.887(2)°, *V* = 746.33(13) Å<sup>3</sup> and *Z* = 6. Unit-cell parameters obtained by the refinement of the powder X-ray diffraction data (Table 6) are: *a* = 10.842(13), *b* = 11.185(11), *c* = 6.463(7) Å; β = 108.81(6)°, *V* = 741.9(2) Å<sup>3</sup> and *Z* = 6. Single-crystal X-ray data collection and structure refinement details for zaykovite are summarised in Table 7. Fractional atomic coordinates and displacement parameters in the crystal structure of the mineral are given in Table 8. Selected interatomic bond lengths are presented in Table 9. Zaykovite is a selenium-dominant analogue of kingstonite, Rh<sub>3</sub>S<sub>4</sub> (Stanley *et al.*, 2005), and the synthetic kingstonite counterpart (Beck and Hillbert, 2000) (Table 10). Despite the Rh–Se system being characterised with a wide range of compositions (Rummery and Heyding, 1967), the synthetic analogue of zaykovite, Rh<sub>3</sub>Se<sub>4</sub> has not yet been reported. Therefore, the discovery of zaykovite is a contribution to the crystal chemistry of the Rh–Se system, which now includes six structurally confirmed

**Table 10.** Comparative crystallographic data for zaykovite, kingstonite and synthetic Rh<sub>3</sub>S<sub>4</sub>.

Mineral	Zaykovite	Kingstonite	Synthetic Rh <sub>3</sub> S <sub>4</sub>
Ideal formula	Rh <sub>3</sub> Se <sub>4</sub>	Rh <sub>3</sub> S <sub>4</sub>	Rh <sub>3</sub> S <sub>4</sub>
Crystal system	Monoclinic	Monoclinic	Monoclinic
Space group	<i>C2/m</i>	<i>C2/m</i>	<i>C2/m</i>
<i>a</i> (Å)	10.8769(11)	10.4616(5)	10.29(2)
<i>b</i> (Å)	11.1921(11)	10.7527(5)	10.67(1)
<i>c</i> (Å)	6.4796(6)	6.2648(3)	6.212(8)
β (°)	108.887(2)	109.000(5)	107.70
<i>V</i> (Å <sup>3</sup> )	746.33(13)	666.34(1)	649.8(1)
<i>d</i> <sub>calc.</sub> (g/cm <sup>3</sup> )	8.32	7.52	6.70
Reference	This work	Stanley <i>et al.</i> (2005)	Beck and Hillbert (2000)

**Table 11.** Minerals and structurally confirmed synthetic compounds in the systems Rh–Se and Rh–S.

X:Rh*	Rh–Se system		Rh–S system		Structure type	References
	Mineral	Ideal formula	Mineral			
2 $\frac{3}{4}$		Rh <sub>3</sub> Se <sub>8</sub>			Rh <sub>3</sub> Te <sub>8</sub>	Kjekshus <i>et al.</i> (1979)
2		RhSe <sub>2</sub>	RhS <sub>2</sub>		Pyrite	Kjekshus <i>et al.</i> (1979); Thomassen (1929)
1 $\frac{1}{2}$	Zaykovite	Rh <sub>2</sub> Se <sub>3</sub>	Rh <sub>2</sub> S <sub>3</sub>	Bowieite	Rh <sub>2</sub> S <sub>3</sub>	Parthe <i>et al.</i> (1967); Desborough and Criddle (1984)
1 $\frac{1}{3}$		Rh <sub>3</sub> Se <sub>4</sub>	Rh <sub>3</sub> S <sub>4</sub>	Kingstonite	Rh <sub>3</sub> S <sub>4</sub>	This work; Beck and Hillbert (2000); Stanley <i>et al.</i> (2005)
1		RhSe			NiAs	Rummery and Heyding (1967)
0.88		Rh <sub>17</sub> Se <sub>15</sub>	Rh <sub>17</sub> S <sub>15</sub>	Miassite	Pd <sub>17</sub> Se <sub>15</sub>	This work; Schubert (1977); Geller (1967); Britvin <i>et al.</i> (2001)

\*Atomic ratios; X = Se or S.

phases (Table 11). As expected, the compounds in this system have many structural analogues in the closely related Rh–S join (Table 11), however the selenide part is more diverse. The pyrite-

type RhX<sub>2</sub> phases (X = Se or S) are known in both systems (Thomassen, 1929; Rummery and Heyding, 1967; Kjekshus *et al.*, 1979), whereas Rh<sub>3</sub>Se<sub>8</sub>, with a rhombohedrally distorted pyrite structure (Kjekshus *et al.*, 1979), has no sulfide analogue. The same is true for RhSe, which adopts a hexagonal close-packed nickeline structure (Rummery and Heyding, 1967), but its sulfide analogue has not been reported.

Zaykovite, as well as kingstonite, have an X:Rh ratio intermediate between that of bowieite, Rh<sub>2</sub>S<sub>3</sub>, and miassite, Rh<sub>17</sub>S<sub>15</sub> (Table 11). Beck and Hillbert (2000), who provided a detailed description of the crystal structure of synthetic Rh<sub>3</sub>S<sub>4</sub> (a kingstonite analogue), showed that it has similarities to the structures of Rh<sub>2</sub>S<sub>3</sub> and Rh<sub>17</sub>S<sub>15</sub>. We highlight the main features of the zaykovite structure, which has the same topology as Rh<sub>3</sub>S<sub>4</sub> and kingstonite, except for the longer Rh–X bond distances due to the domination of Se in the X sites (Table 9). Of four symmetrically independent Rh sites, Rh3 and Rh4 are each coordinated by 6 Se atoms to form distorted octahedra [RhSe<sub>6</sub>], similar to those in synthetic Rh<sub>2</sub>Se<sub>3</sub> (Parthe *et al.*, 1967). The [RhSe<sub>6</sub>] octahedra are connected via common edges to form 6-membered rings (Fig. 6a). The coordination of Rh1 and Rh2 sites is more complex – besides Se atoms, each of them is bonded to another Rh atom to form Rh–Rh bonds (Table 9), that results in the creation of the [Rh<sub>6</sub>] puckered rings with chair-like conformation (Fig. 6b). It is noteworthy that the domains formed by metallic-type Rh–Rh bonds similar to those in zaykovite were reported in Rh<sub>17</sub>S<sub>15</sub> – a synthetic analogue of miassite (Schubert, 1977; Britvin *et al.*, 2001). The [Rh<sub>6</sub>] puckered rings in the zaykovite structure are arranged into the infinite framework via Se4–Se4 diselenide (pyrite-type) ‘dumbbell’ bridges (Fig. 6b). The Se4–Se4 distance in the ‘zaykovite dumbbell’ is 2.409 Å, which is, taking into account partial substitution of Se for S, almost the same as 2.499 Å in pyrite-type RhSe<sub>2</sub> (Kjekshus *et al.*, 1979).

The EBSD pattern of zaykovite (Fig. 7a) is well resolved by the theoretical structure of kingstonite (AMCSD 0014575) with a MAD of 0.37° on the basis of maximum of 12 bands (Fig. 7b).

The Kikuchi band contrast shows that zaykovite forms homogeneous grains with a tendency to form euhedral crystals with pronounced crystallographic facets (Fig. 8a). It forms single crystals, elongated along the [001] axis (Fig. 8b, 9b). The holotype crystal consists of two blocks, in which orientation differs by 5.5° (Fig. 8c).

An unexpected result was obtained through EBSD mapping of an area that contains several grains of zaykovite and a Pd–Sb–Te phase in a Pt–Fe alloy matrix (Fig. 9). Pd–Sb–Te phase grains have a chaotic orientation typical of late inclusions, however three zaykovite grains in two different platinum subgrains have the same orientation. The only viable explanation except accidental coincidence is that formation of zaykovite precedes

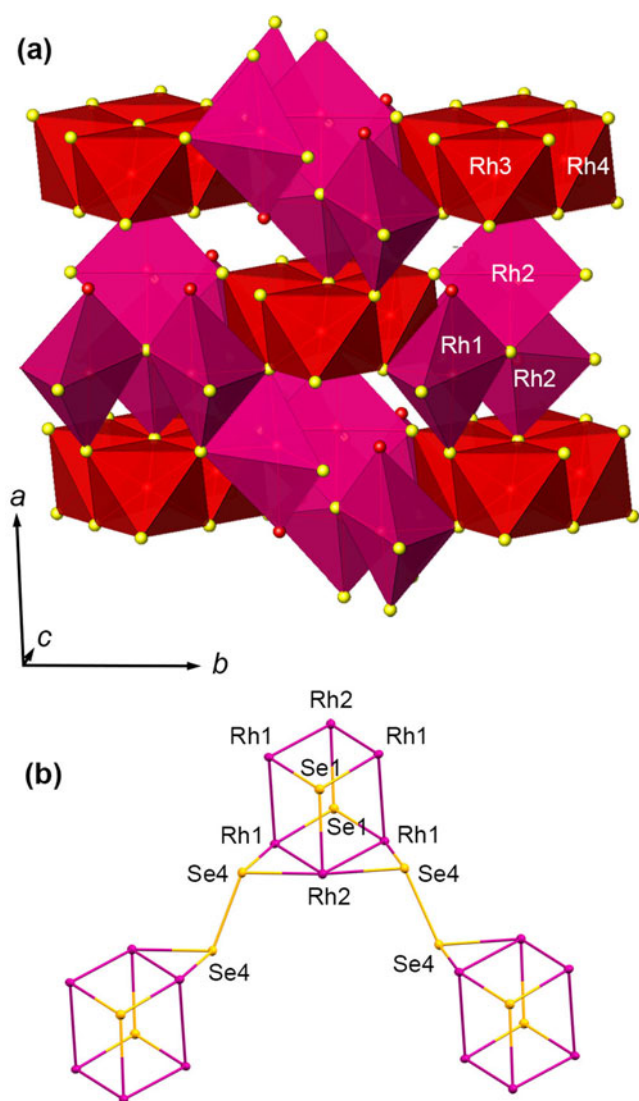


**Fig. 6.** The crystal structure of zaykovite. (a) Polyhedral representation; a three-dimensional framework composed of two cluster types: (1) Clusters of corner-sharing [Rh(RhSe<sub>4</sub>)] and [RhSe<sub>5</sub>] distorted square pyramids (coordination around Rh1 and Rh2 atoms) and (2) Clusters of edge-sharing octahedra [RhSe<sub>6</sub>] (around Rh3 and Rh4 atoms). (b) Ball-and-stick representation of six-membered Rh1-Rh2 clusters, which form pseudo-cubic cages together with Se1 atoms. These clusters are connected in a framework via Se4–Se4 diselenide (pyrite-type) dumbbells. The scale and orientation of structural fragments is the same in (a) and (b).



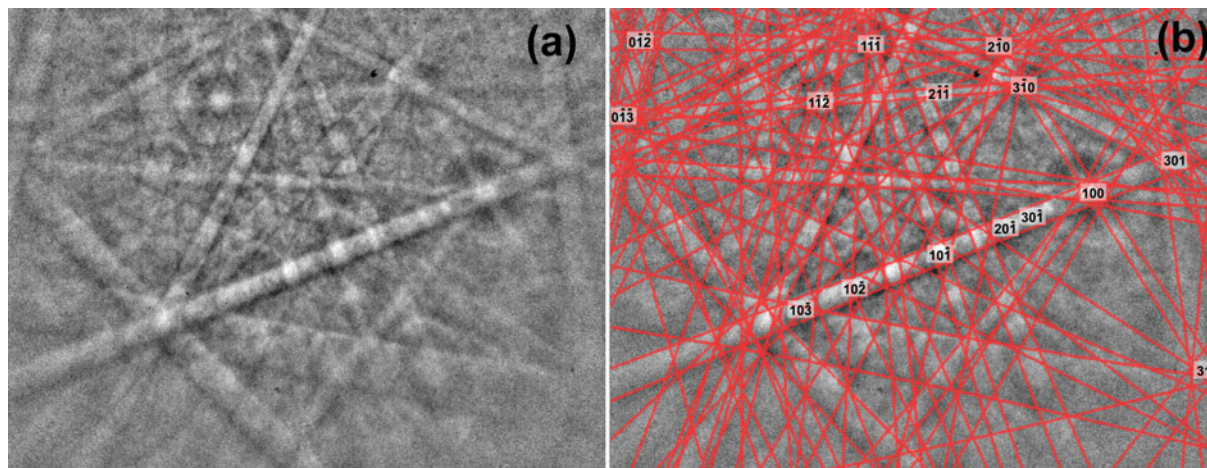


**Fig. 7.** EBSD pattern of (a) zaykovite and (b) the theoretical kingstonite solution fitted over the pattern.

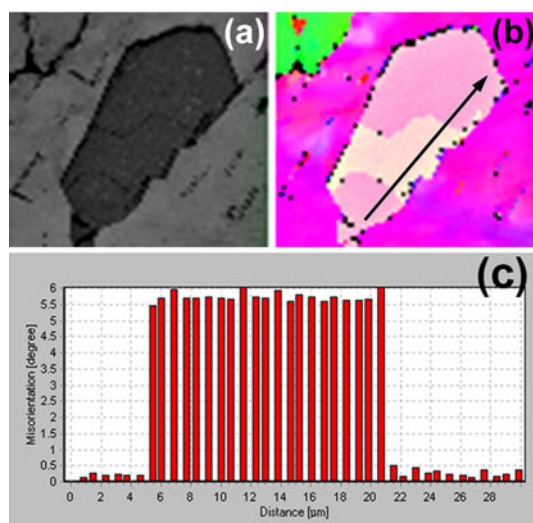


**Fig. 8.** (a) Band contrast, (b) orientation in Euler colours, and (c) misorientation profile of the holotype zaykovite crystal. Line of the profile is shown in (b).

crystallisation of the Pt–Fe alloy and zaykovite inherits the primary orientation of a protophase. Also, the zaykovite grains manifest ductility, that is seen on the misorientation map as a gradual colour change from the point where the grain contacts with the distorted bands in the Pt–Fe alloy. Unfortunately, a potential correlation between zaykovite distortion and distortion of the Pd–Sb–Te phase, as well as their host Pt–Fe alloy cannot be resolved because of the high degree of surface distortion during polishing.

## Discussion

### Chemical composition

The chemical composition of selenium-bearing rhodium-dominant sulfide inclusions in Pt–Fe alloy grains of the Kazan placer was analysed using energy dispersive spectroscopy (EDS). (Table 4). The negative correlation between S and Se contents in these inclusions indicates a continuous isomorphic series between kingstonite and zaykovite (Fig. 10).

### Origin of the zaykovite

The sources of gold in the placer probably were gold–sulfide and gold–quartz occurrences in the Lower Carboniferous sedimentary rocks, represented by carbonaceous and clayey shale, siltstone and limestone. Only the Tambov vein-disseminated gold–sulfide–quartz ore deposit is known in the vicinity of the placer (Podkorytov, 2001).

Sources of PGM may be the Varshav and Mogutovsky serpentinised dunite–harzburgite massifs, as well as the Gogino gabbro–pyroxenite–dunite zoned massif (Zaykov *et al.*, 2018). However, the finds of laurite, iridium sulfide close to kashinite, and unspecified iridium arsenide were described only for the Vladimir chromite deposit located in the Varshavka massif (Zaykov *et al.*, 2012, 2018; Ankushev *et al.*, 2016). It has been suggested that the eroded ultramafic massif or its upper part may also be a source of PGM in the Kazan placer.

At present, it is proposed that minerals of the laurite–erlichmanite series, kashinite and some PGE thiospinels are formed at the late stage of magmatic crystallisation of PGM in the ultramafic massif (Tolstykh *et al.*, 2011, 2015; Mochalov, 2013). The absence of a Se and Rh admixture in the Pt–Fe alloy (Artenm'ev and Zaykov, 2018) suggests, that the presence of selenides is not the result of solid-solution decomposition.

Based on the euhedral form of the inclusions of bowieite–kashinite and cuprorhodsites in early-formed Pt–Fe alloy grains, their crystallisation from melt during the early magmatic stages has been suggested (Zaccarini *et al.*, 2016; Stepanov *et al.*, 2020). The thermodynamic advantage of crystallisation of  $Rh_3S_4$  in terms of the Gibbs energy minimisation in comparison with phases with other Rh:S ratios has been proven experimentally (Jacob and Gupta, 2014). The crystallochemical similarity of selenium and sulfur suggests a similar tendency for rhodium selenides.

The crystallisation of native osmium, iridium and laurite from a melt has been confirmed experimentally (Brenan and Andrews, 2001). The pronounced euhedral shape of zaykovite indicates its crystallisation before or coevally with the Pt–Fe alloy. The identical orientations of zaykovite crystals hosted in the different Pt–Fe alloy subgrains also favour the early magmatic crystallisation hypothesis, assuming that the trapped Os lamellae (Fig. 3) represent the earliest magmatic phase.

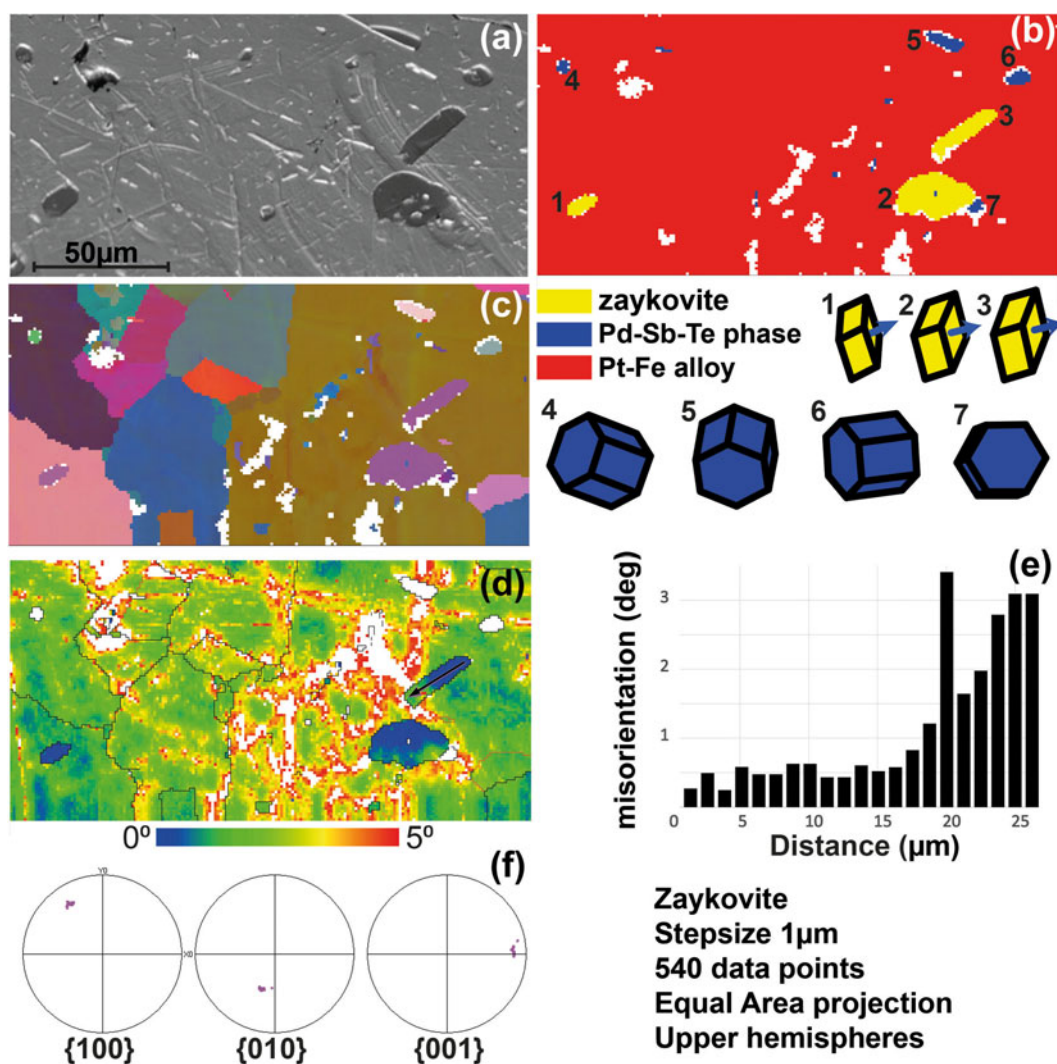


**Fig. 9.** BSE image (a), phase distribution with orientation of the zaykovite and Pd-Sb-Te grains, blue arrow shows [001] axis of zaykovite (b), and EBSD maps (c–d) of Pt-Fe alloy matrix containing zaykovite and mertieite in Euler angles colour scheme with zaykovite cell orientations (c), grains boundaries (d), misorientations profile of the zaykovite grain No.3 (e), and pole figures for zaykovite grains (f).

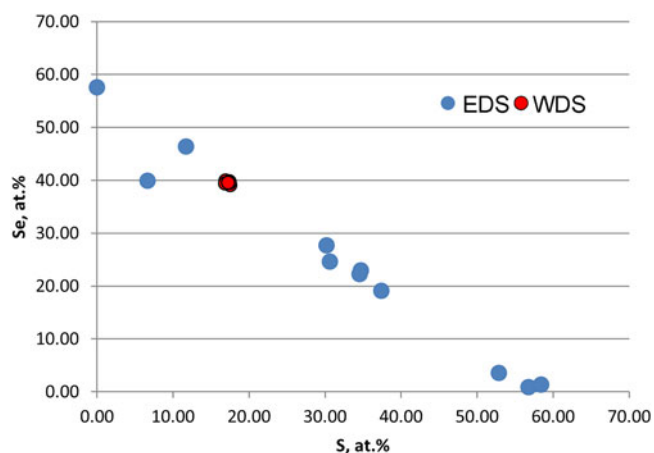


**Fig. 10.** S-Se plot for the zaykovite-kingstonite series for specimens from the Kazan placer.

**Conclusion**

Zaykovite, ideally  $Rh_3Se_4$  was found as inclusions in Pt-Fe alloy grains in heavy mineral concentrates of the Kazan gold placer

(South Urals). Zaykovite forms crystals up to 40 μm in size inter-grown with an unnamed Pd-Sb-Te phase and Au-Pd alloy. Its empirical formulae is  $(Rh_{2.26}Pt_{0.46}Ir_{0.25}Ru_{0.01}Pd_{0.01}Fe_{0.01})_{\Sigma 3.00}(Se_{2.77}S_{1.21}Te_{0.02})_{\Sigma 4.00}$ . The mineral is grey with black streak and has a metallic lustre. It is the Se analogue of kingstonite with the monoclinic structure and space group C2/m. The crystal structure was solved using single-crystal diffraction data. Unit-cell parameters are  $a = 10.877(1)$ ,  $b = 11.192(1)$ ,  $c = 6.4796(6)\text{Å}$  and  $\beta = 108.887(2)$ . The composition of the studied inclusions in the Pt-Fe alloy grains indicates the existence of a continuous kingstonite-zaykovite series. The Varshavka and Mogutovsky serpentinised dunite-harzburgite massifs, as well as the Gogino gabbro-pyroxenite-dunite zoned massif could be sources of PGM including zaykovite in the Kazan placer. The euhedral habit of zaykovite points to its probable crystallisation before or simultaneously with Pt-Fe alloy, although slightly later than native osmium.

**Acknowledgements.** The authors are grateful to A.Yu. Ivanov and B.Ya. Hismatullin (“Miasskiy Priisk”) for heavy mineral concentrates from the Kazan placer, Maksim Lozhkin (Nanophotonics Resource Center, SPSU) for preparation of the sample surface for EBSD mapping and the Geomodel

Resource Center for making the EBSD analysis possible. We also thank Marina Yudovskaya, Oleg Siida, an anonymous reviewer and Associate Editor Frantisek Laufek for the fruitful comments and linguistic corrections. The work was supported by state contract no. 075-00880-22-00.

**Competing interests.** The authors declare none.

**Supplementary material.** To view supplementary material for this article, please visit <https://doi.org/10.1180/mgm.2022.122>

## References

- Ankushev M.N., Zaykov V.V., Kotlyarov V.A. and Romanenko M.E. (2016) Chrome spinels and accessory mineralization in the weathering crust of the Vladimir Deposit, Varshavsky Ultramafic Massif, Southern Urals. *Geology of Ore Deposits*, **58**, 697–710.
- Artem'ev D.A. and Zaykov V.V. (2018) Impurity elements in the native platinum from placers, ICP-MS-LA analysis results. *Geoarchaeology and archaeological mineralogy-2018: Conference materials*, pp 161–164 [in Russian].
- Bai W., Tao S., Yang J., Fang Q., Shi N. and Li G. (2007) A mineral assemblage of sulfides and sulfo-arsenides from the ophiolite mantle in Tibet. *Acta Petrologica et Mineralogica*, **26**, 418–428 [in Chinese].
- Barkov A.Y., Nikiforov A.A., Tolstykh N.D., Shvedov G.I. and Korolyuk V.N. (2017) Compounds of Ru-Se-S, alloys of Os-Ir, framboidal Ru nanophases, and laurite-clinoclone intergrowths in the Pados-Tundra complex, Kola Peninsula, Russia. *European Journal of Mineralogy*, **29**, 613–621.
- Barkov A.Y., Nikiforov A.A., Barkova L.P., Korolyuk V.N. and Martin R.F. (2021) Zones of PGE-chromite mineralization in relation to crystallization of the Pados-Tundra Ultramafic Complex, Serpentinite Belt, Kola Peninsula, Russia. *Minerals*, **11**, 68, <https://doi.org/10.3390/min11010068>.
- Beck J. and Hillbert T. (2000) Ein ‚altes‘ Rhodium sulfid mit überraschender Struktur: Synthese, Kristallstruktur und elektronische Eigenschaften von  $Rh_3S_4$ . *Zeitschrift für anorganische Chemie*, **626**, 72–79.
- Beginov V.D. and Zav'yalov E.N. (2016) Ferhodsit (Fe, Rh, Ir, Ni, Cu, Co, Pt)<sub>9-x</sub>S<sub>8</sub>, a new mineral from the Nizhnii Tagil ultrabasic massif. *Novye Dannye o Mineralakh*, **51**, 8–11 [in Russian].
- Belogub E.V., Zaykova E.V., Kotlyarov V.A., Shilovskikh V.V., Britvin S.N. and Pautov L.A. (2019) Selenium in the minerals of the platinum group minerals from gold placer of the South Urals. *Mineralogical museums: Conference material. Sain-Petersburg*, SPbU. 87–89 [in Russian].
- Belogub E.V., Britvin S.N., Shilovskikh V.V., Pautov L.A., Kotlyarov V.A. and Zaykova E.V. (2020) Zaykovite, IMA 2019-084. CNMNC Newsletter No. 54. *Mineralogical Magazine*, **84**, <https://doi.org/10.1180/mgm.2020.21>
- Brenan J. and Andrews D. (2001) High-temperature stability of laurite and Ru–Os–Ir alloy and their role in PGE fractionation in mafic magmas. *The Canadian Mineralogist*, **39**, 341–360.
- Britvin S.N., Rudashevsky N.S., Bogdanova A.N. and Shcherbachev D.K. (1998) Polkanovite  $Rh_{12}As_7$  – a new mineral from placers of Miass River, Urals. *Zapiski Vserossiiskogo Mineralogicheskogo Obshchestva*, **127**, 60–62 [in Russian].
- Britvin S.N., Rudashevsky N.S., Bogdanova A.N. and Shcherbachev D.K. (1999) Palladodymite  $(Pd,Rh)_2As$  – a new mineral from placers of Miass River, Urals. *Zapiski Vserossiiskogo Mineralogicheskogo Obshchestva*, **128**, 39–42 [in Russian].
- Britvin S.N., Rudashevsky N.S., Bogdanova A.N. and Shcherbachev D.K. (2001) Miassite  $Rh_{17}S_{15}$  – a new mineral from a placer of Miass River, Urals. *Zapiski Vserossiiskogo Mineralogicheskogo Obshchestva*, **130**, 41–45 [in Russian].
- Britvin S.N., Dolivo-Dobrovolsky D.V. and Krzhizhanovskaya M.G. (2017) Software for processing the X-ray powder diffraction data obtained from the curved image plate detector of Rigaku RAXIS Rapid II diffractometer. *Zapiski Rossiiskogo Mineralogicheskogo Obshchestva*, **146**, 104–107 [in Russian].
- Cabri L. and Feather C. (1975) Platinum-iron alloys: a nomenclature based on a study of natural and synthetic alloys. *The Canadian Mineralogist*, **13**, 117–126.
- Cabri L., Oberthur T. and Schumann D. (2022) The mineralogy of Pt-Fe alloys and phase relations in the Pt-Fe binary system. *The Canadian Mineralogist*, **60**, 331–339.
- Cook N.J., Wood S.A., Gebert W., Bernhardt H.J. and Medenbach, O. (1994) Crerarite, a new Pt-Bi-Pb-S mineral from the Cu-Ni-PGE deposit at Lac Sheen, Abitibi-Temiscamisque, Quebec, Canada. *Neues Jahrbuch für Mineralogie, Monatshefte*, 567–575.
- Davis R.J., Clark A.M. and Criddle A.J. (1977) Palladseite, a new mineral from Itabira, Minas Gerais, Brazil. *Mineralogical Magazine*, **41**, 123.
- Desborough G.A. and Criddle A.J. (1984) Bowieite: a new rhodium-iridium-platinum sulfide in platinum-alloy nuggets, Goodnews Bay, Alaska. *The Canadian Mineralogist*, **22**, 543–552.
- Dolomanov O.V., Bourhis L.J., Gildea R.J., Howard J.A. and Puschmann H. (2009) OLEX2: a complete structure solution, refinement and analysis program, *Journal of Applied Crystallography*, **42**, 339–341.
- Geller S. (1967) The crystal structure of the superconductor  $Rh_{17}S_{15}$ . *Acta Crystallographica*, **15**, 1198–1201.
- Ivanishchev A.V., Sazonov V.N., Savelieva K.P., Barannikov A.G. et al. (2005) Systematization and classification of gold deposits in the Sverdlovsk and Chelyabinsk districts, worked out in previous years, in order to estimation of their prospects and identify objects for involvement to industrial mining. *Unpublished report of LLC "South-Urals geological center"* [in Russian].
- Jacob K.T. and Gupta P. (2014) Gibbs free energy of formation of rhodium sulfides. *The Journal of Chemical Thermodynamics*, **70**, 39–45.
- Jebwab J., Cervelle B., Gouet G., Hubaut X. and Piret P. (1992) The new platinum selenide luberoite  $Pt_5Se_4$  from the Lubero region (Kivu Province, Zaire). *European Journal of Mineralogy*, **4**, 683–692.
- Johan Z., Picot P. and Pierrot R. (1970) L'oosterboschite  $(Pd,Cu)_7Se_5$ , une nouvelle espèce minérale et la trogtalite cupro-palladifère de Musonoi (Katanga). *Bulletin de la Société française de Minéralogie et de Cristallographie*, **93**, 476–481.
- Karimova V., Zolotarev A.A., Evstigneeva T.L. and Johanson B.S. (2018) Mertieite-II,  $Pd_8Sb_{2.5}As_{0.5}$ , crystal-structure refinement and formula revision. *Mineralogical Magazine*, **82**(S1), S247–S257.
- Kjekshus A., Rakke T. and Andresen A.F. (1979) Pyrite like phases in the Rh-Se system. *Acta Chemica Scandinavica*, **A33**, 719–725.
- Krivovichev V.G. (2021) *Mineral Species*. St. Petersburg University Publishing House, Russia, 599 pp. [in Russian].
- Malitch K.N., Stepanov S.Yu., Badanina I.Yu. and Khiller V.V. (2015) Assemblages of platinum-group minerals of the Svetlyi Bor, Veresovi Bor, and Nizhnii Tagil clinopyroxenite–dunite massifs of the Middle Urals. *Vestnik UrO RMO*, **12**, 65–83 [in Russian].
- Mason J. and Schuh C. (2009) Representations of texture. Pp 35–51 in: *Electron Backscatter Diffraction in Materials Science* (Schwartz A.J., Kumar M., Adams B.L. and Field D.P., editors). Springer.
- Mochalov A.G. (2013) A genetic model of PGM hosted in cumulative gabbro-pyroxenite–dunite complexes of the Koryak Highland, Russia. *Geology of Ore Deposits*, **55**, 145–161.
- Paar W.H., Roberts A.C., Criddle A.J. and Topa D. (1998) A new mineral, chrisstanleyite,  $Ag_2Pd_3Se_4$ , from Hope's Nose, Torquay, Devon, England. *Mineralogical Magazine*, **62**, 257–264.
- Palamarchuk R.S., Stepanov S.Yu., Kozlov A.V., Khanin D.A., Varlamov D.A., Zolotarev A.A., Jr., Kiseleva D.V. and Shilovskikh V.V. (2020) Platinum-group minerals from the Malaya Kamenushka River placer, Middle Urals, Russia. *Mineralogical Magazine*, **84**, 900–912.
- Parthe E., Hohnke D. and Hulliger F. (1967) A new structure type with octahedron pairs for  $Rh_2S_3$ ,  $Rh_2Se_3$  and  $Ir_2S_3$ . *Acta Crystallographica*, **23**, 832–840.
- Podkorytov, P.P. (2001) *Report on geological work at the Tambov gold deposit conducted by Kochkarsky GGP in 1991–1992 and OOO (limited company) Bredinskaya Gold Mining Company in 1995–2001* [in Russian].
- Polekhovskiy Y.S., Tarasova I.P., Nesterov A.P., Pakhomovskiy Y.A. and Bakhchisaraitsev A.Y. (1997) Sudovikovite  $PtSe_2$  – a new platinum selenide from Karelia metasomite. *Doklady Akademii Nauk*, **354**, 82–85 [in Russian].
- Rakhimov I.R., Saveliev D.E., Salikhov D.N., Vishnevskiy A.V. and Vladimirov A.G. (2021a) Multi-stage magmatic-hydrothermal sulfide-PGE mineralization of the Khudolaz complex (South Urals). *Geology of Ore Deposits*, **63**, 341–367.

- Rakhimov I.R., Saveliev D.E. and Vishnevskiy A.V. (2021b). Platinum metal mineralization of the South Urals magmatic complexes: geological and geodynamic characteristics of formations, problems of their genesis, and prospects. *Geodynamics and Tectonophysics*, **12**, 409–434 [in Russian].
- Roberts A.C., Paar, W.H., Cooper, M.A., Topa, D., Criddle, A.J. and Jedwab, J. (2002) Verbeekite, monoclinic PdSe<sub>2</sub>, a new mineral from the Musonoi Cu-Co-Mn-U mine, near Kolwezi, Shaba Province, Democratic Republic of Congo. *Mineralogical Magazine*, **66**, 173–179.
- Rummery T.E. and Heyding R.D. (1967) The rhodium/selenium system. *Canadian Journal of Chemistry*, **45**, 131–137.
- Saveliev D.E., Zaykov V.V., Kotlyarov V.A., Zaykova E.V. and Kraynev Yu.D. (2017) Chromites and accessory minerals in chromitites and ultramafic rocks of the Nurali massif (the South Urals). *Zapiski RMO*, **1**, 59–84 [in Russian].
- Schubert K. (1977) On the binding in phases of T<sup>10</sup>-B<sup>6</sup> mixtures. *Acta Crystallographica*, B33, 2631–2639.
- Sheldrick G.M. (2015) Crystal structure refinement with SHELXL. *Acta Crystallographica*, C71, 3–8.
- Stanley C.J., Criddle A.J., Spratt J., Roberts A.C., Szymanski J.T. and Welch M.D. (2005) Kingstonite, (Rh,Ir,Pt)<sub>3</sub>S<sub>4</sub>, a new mineral species from Yubdo, Ethiopia, Locality: Bir River, Yubdo District, Wallaga Province, Ethiopia. *Mineralogical Magazine*, **69**, 447–453.
- Stepanov S.Yu., Palamarchuk R.S., Kozlov A.V., Khanin D.A., Varlamov D.A. and Kiseleva D.V. (2019) Platinum-group minerals of Pt-placer deposits associated with the Svetloborsky Ural-Alaskan Type Massif, Middle Urals, Russia. *Minerals*, **9**, 77, <https://doi.org/10.3390/min902007>
- Stepanov S.Yu., Palamarchuk R.S., Antonov A.V., Kozlov A.V., Varlamov D.A., Khanin D.A. and Zolotarev A.A., Jr. (2020) Morphology composition, and ontogenesis of Platinum-Group Minerals in chromitites of zoned clinopyroxenite–dunite massifs of the Middle Urals. *Russian Geology and Geophysics*, **61**, 47–67.
- Thomassen L. (1929) Über Kristallstrukturen einiger binärer Verbindungen der Platinmetalle II. *Zeitschrift für Physikalische Chemie*, **B4**, 277–287.
- Tolstykh N.D., Telegin Yu.M. and Kozlov A.P. (2011) Platinum mineralization of the Svetloborsky and Kamenushinsky massifs (Urals Platinum Belt). *Russian Geology and Geophysics*, **52**, 603–619.
- Tolstykh N., Kozlov A. and Telegin, Yu. (2015). Platinum mineralization of the Svetly Bor and Nizhny Tagil intrusions, Urals Platinum Belt. *Ore Geology Reviews*, **67**, 234–243.
- Vymazalová A., Laufek F., Drábek M., Cabral A.R. Haloda J., Sidorinová T., Lehmann B., Galbiatti H.F. and Drahokoupil J. (2012) Jacutingaite, Pt<sub>2</sub>HgSe<sub>3</sub>, a new platinum-group mineral species from the Cauê iron-ore deposit, Itabira district, Minas Gerais, Brazil. *The Canadian Mineralogist*, **50**, 431–440.
- Zaccarini F., Bindi L., Pushkarev E., Garuti G. and Bakker R.J. (2016) Multi-analytical characterization of minerals of the bowieite-kashinite series from the Svetly Bor complex, Urals, Russia, and comparison with worldwide occurrences. *The Canadian Mineralogist*, **54**, 461–473.
- Zaykov V.V., Samoilo O.V., Yuminov A.M. and Belogub E.V. (2011) Laurite and native gold in chromium ores of the Varshavskoe ore field (South Urals). *Mineralogy of Urals: Conference materials*, 108–111 [in Russian].
- Zaykov V.V., Savel'ev D.E., Kotlyarov V. A., Yuminov A. M., Zherebtcov D.A., Galimov D.M. and Sudarikov M.V. (2012) Platinoids in the chromite ores of the South Urals: data on Karabash, Varshavka and Middle Kraka ultramafic massifs. *Metallogeny of the Ancient and Modern Oceans*, **18**, 176–182 [in Russian].
- Zaykov V.V., Melekestseva I.Yu., Zaykova E.V., Kotlyarov V.A. and Kraynev Yu.D. (2017) Gold and platinum group minerals in placers of the South Urals: Composition, microinclusions of ore minerals and primary sources. *Ore Geology Reviews*, **85**, 299–320.
- Zaykov V.V., Savel'ev D.E. and Zaykova E.V. (2018) The nature of microinclusions of chromespinels in minerals of PGE from the gold placers of South Urals. *Notes of the All-Russian Mineralogical Society*, **147**, 27–40 [in Russian].
- Zaykova E.V., Blinov I.A. and Kotlyarov V.A. (2020) Mineral inclusions in the platinum grains from the Kazan placer (South Urals). *Mineralogy*, **6**, 33–46 [in Russian].